Chemosphere 256 (2020) 127050

Contents lists available at ScienceDirect

Chemosphere

journal homepage: www.elsevier.com/locate/chemosphere

ROS-generation potential of Humic-like substances (HULIS) in ambient $PM_{2.5}$ in urban Shanghai: Association with HULIS concentration and light absorbance

Xiaoya Xu [a], Xiaohui Lu [a, *], Xiang Li [a], Yaxi Liu [a], Xiaofei Wang [a], Hong Chen [a], Jianmin Chen [a], Xin Yang [a, b, **], Tzung-May Fu [c], Qianbiao Zhao [a, d], Qingyan Fu [d]

[a] Shanghai Key Laboratory of Atmospheric Particle Pollution and Prevention, Department of Environmental Science and Engineering, Fudan University, Shanghai, 200433, China
[b] Shanghai Institute of Pollution Control and Ecological Security, Shanghai, 200092, China
[c] School of Environmental Science and Engineering, Southern University of Science and Technology, Shenzhen, Guangdong Province, China
[d] Shanghai Environmental Monitoring Center, Shanghai, 200235, China

HIGHLIGHTS

- HULIS with high ROS-generation potential were observed at low $PM_{2.5}$ concentration.
- High-ROS/Low-Conc HULIS were likely formed via aqueous-phase reactions.
- HULIS with higher ROS-generation potential showed stronger light absorbance.

ARTICLE INFO

Article history:
Received 30 January 2020
Received in revised form
7 May 2020
Accepted 9 May 2020
Available online 13 May 2020

Handling Editor: Hongliang Zhang

Keywords:
Reactive oxygen species (ROS)
Humic-like substances (HULIS)
$PM_{2.5}$
Light absorbance
Surrogate lung fluid (SLF)

ABSTRACT

Ambient fine particulate matter ($PM_{2.5}$) can cause adverse health effects through the generation of reactive oxygen species (ROS) after inhalation. Humic-like substances (HULIS) are major constituents contributing to the ROS-generation potential in organic aerosols. In this study, $PM_{2.5}$ samples in urban Shanghai during autumn and winter (2018–2019) were collected. Mass-normalized ·OH generation rate in surrogate lung fluid (SLF) was used to denote the intrinsic ROS-generation potential of $PM_{2.5}$ or of the HULIS isolated from $PM_{2.5}$. In this study, ROS-generation potential of $PM_{2.5}$ decreased with increasing ambient $PM_{2.5}$ concentration due to higher percentage of inorganic components in high $PM_{2.5}$ event. Same trend was observed for the ROS-generation potential of unit mass of HULIS, which was higher when HULIS and $PM_{2.5}$ concentrations were both relatively lower. The HULIS with high ROS-generation potential but low concentration (High-ROS/Low-Conc HULIS) were likely produced by the atmospheric aqueous-phase reactions during nighttime or under high relative humidity conditions, not from biomass burning emissions or the photochemical pollution products. The association between ROS-generation potential and light absorption properties of HULIS was studied as well. The High-ROS/Low-Conc HULIS also showed stronger light absorbance than the other HULIS. Our results implied the potentially important roles that HULIS species might play in atmospheric environment and human health even when the $PM_{2.5}$ pollution is low.

1. Introduction

The adverse health effects by atmospheric fine particulate matter ($PM_{2.5}$) have been well documented in epidemiologic and toxicological studies (Pope et al., 2004; Delfino et al., 2005; Brook et al., 2010; Ito et al., 2011; Huang et al., 2018). A key mechanism to explain the adverse health effects involves the generation of reactive oxygen species (ROS, e.g. ·OH, H_2O_2) by inhaled $PM_{2.5}$,

* Corresponding author.
** Corresponding author. Shanghai Key Laboratory of Atmospheric Particle Pollution and Prevention, Department of Environmental Science and Engineering, Fudan University, Shanghai, 200433, China.
E-mail addresses: luxiaohui@fudan.edu.cn (X. Lu), yangxin@fudan.edu.cn (X. Yang).

https://doi.org/10.1016/j.chemosphere.2020.127050
0045-6535/

since excessive ROS can lead to oxidative stress in vivo (Tao et al., 2003; Mudway et al., 2004; See et al., 2007). Thus, the ROS-generation potential, also termed as oxidative potential, is a characterization of the toxicity of particulate matter. In the past decades, many acellular methods have been developed and employed to measure the ROS-generation potential of $PM_{2.5}$ (Charrier and Anastasio, 2011; Hedayat et al., 2015; Yu et al., 2020). These acellular methods can be outlined as measuring the depletion of the reducing reagent or the production of ROS in aqueous solution or in a pulmonary epithelial lining fluid (Bates et al., 2019). For example, dithiothreitol (DTT) is a typical proxy for cellular reductants, so the DTT loss rate in a mixture solution with $PM_{2.5}$ extracts is representative for the ROS-generation potential by particulate matter (Cho et al., 2005; Charrier and Anastasio, 2012). Likewise, the depletion of some antioxidants (e.g., ascorbic acid, glutathione) can be the indicators to quantify the ROS-generation (Godri et al., 2011; Visentin et al., 2016). Different from the DTT assay, the antioxidants assays are generally performed in the surrogate lung fluid (SLF). Another category of acellular methods involves direct measurement of some special ROS (Charrier et al., 2014; Charrier and Anastasio, 2015). The production rate of ·OH in SLF, for example, is often used as an index for ROS-generation potential determination (Vidrio et al., 2008, 2009). The ·OH quantification can be obtained by using some fluorescent molecular probes, and disodium terephthalate (TPT) was considered as the most applicable probe according to Son et al. (2015)'s work. Besides, since DTT consumption is mainly triggered by H_2O_2 rather than ·OH, measurement of ·OH production rate was recently proposed as a necessary complement in the DTT assay (Xiong et al., 2017).

Despite the various acellular methods, there is yet no consensus reached for which is the best method. Our literature survey indicates the DTT assay as the most widely-used, but a certain number of studies upon spatiotemporal assessment for the aerosol ROS-generation potential have been based on the ·OH measurement in the SLF. Shen and Anastasio (2011) measured the ·OH generation by particles in San Joaquin Valley of California. Ma et al. (2015) analyzed the production of ·OH from Fe-containing $PM_{2.5}$ in Guangzhou, China. Li et al. (2019a) recently studied the association between ·OH generation and the $PM_{2.5}$ concentration in North China Plain.

$PM_{2.5}$ constituents are usually complicated. The effects of $PM_{2.5}$ components on the ROS-generation potential could be varied for different assays, but some observations were similar. Both the DTT assays and ·OH measurements demonstrated that quinones and transition metals are the typical ROS-generating components in $PM_{2.5}$ (Charrier et al., 2014, 2015; Charrier and Anastasio, 2012, 2015; Lyu et al., 2018). The organic-metal complexation occurs to have metal-specific influence upon not only the DTT activities (Lin and Yu, 2019; Lu et al., 2019) but the ·OH production in SLF (Charrier and Anastasio, 2011; Lin et al., 2012; Wei et al., 2019) as well. For the organic carbon (OC) in aerosols, except for acting as metal chelators to enhance the metals' potential of ROS-generation, the organics themselves (including but not limited to quinones) could be the contributors. Some studies on secondary organic aerosols (SOA) indicate that some unidentified SOA constituents beyond quinone-derived SOA can be also redox active (McWhinney et al., 2013; Tuet et al., 2017). Reduced N-containing heterocyclic compounds (e.g., imidazole, pyridine and their derivatives) among aqueous SOA, despite their negative DTT activity, can enhanced the ROS production of quinones via the H-bonding formation (Dou et al., 2015). Water-soluble organic carbon (WSOC), especially the hydrophobic sub-fraction of WSOC, was reported to dominate the ROS-generation potential of organic aerosols (Verma et al., 2012; Chen et al., 2019).

Humic-like substances (HULIS) refer to a special class of species that can be chromatographically fractionated from WSOC in ambient aerosols (Varga et al., 2001; Zheng et al., 2013). They are usually high-molecular-weight and have complicated chemical structures (Stone et al., 2009; Lin et al., 2012; Chen et al., 2016). HULIS species have major contribution to the light absorbance of water-soluble brown carbon in atmosphere (Fan et al., 2016; Wu et al., 2018). They have also been recognized as major redox-active species that can serve as electron carriers to promote ROS formation (Lin and Yu, 2011). HULIS with higher polarity were demonstrated to have higher DTT activity (Verma et al., 2015). Another DTT assay based study indicated that HULIS alone may produce even higher ROS-generation potential than their iron complexes (Lu et al., 2019). Emission sources and aging processes may also have influence on the ROS-generation by HULIS. According to the researches by Ma et al. (2018, 2019), the secondary HULIS were reported to dominate the ROS-generation potential of HULIS in $PM_{2.5}$ in Beijing while in Hong Kong, biomass burning related HULIS transported from polluted Pearl River Delta region were found to have the significant ROS activity. Though the above studies all involved the DTT assays, a few laboratory studies on HULIS were performed by using ·OH measurement in SLF (Gonzalez et al., 2017; Wei et al., 2019). A very recent report also shows the well correlation between the HULIS ROS-generation potential measured by ascorbic acid assay and by ·OH measurement in SLF (Lin and Yu, 2020). Moreover, the reported studies on HULIS, whichever assays were applied, have mainly focused on the pollution events or particular sources for HULIS. Few has studied the ROS-generation by HULIS at the low $PM_{2.5}$ concentration in less-polluted periods.

In this work, we focused on the mass-normalized ROS-generation potential of HULIS and its association with HULIS concentration, aiming to explore the potential toxicity of HULIS at different levels of $PM_{2.5}$ pollution in the urban atmosphere. $PM_{2.5}$ samples in urban Shanghai were collected and the major chemical components were characterized. HULIS species were then isolated from the $PM_{2.5}$ samples, and then underwent the reaction in SLF. The ·OH generation rate was measured to represent the ROS-generation potential. In this way, the potential interactions between HULIS and other aerosol components to affect ROS-generation were excluded. The HULIS, especially at low $PM_{2.5}$ concentration (when HULIS concentration was also low), were assessed for their possible source and oxidative potential. Furthermore, the light absorbance of HULIS at low or high $PM_{2.5}$ concentration was analyzed.

2. Material and methods

2.1. Aerosol sampling and chemical analyzing

Ambient aerosol sampling was carried out at the Jiangwan campus of Fudan University (located in the northeast of urban Shanghai) in autumn and winter (from September 29, 2018 to January 4, 2019). The meteorological parameters during the sampling periods were obtained from a meteorological website (http://meteomanz.com). Online $PM_{2.5}$ and O_3 concentrations were monitored by a Tapered Element Oscillating Microbalance with Filter Dynamic Measurement System (TEOM-FDMS, 1405-F) and a O_3 analyzer (TEI 49i), respectively. The fire hotspots data were obtained from MODIS satellite-based fire count data (https://firms.modaps.eosdis.nasa.gov/map/), and the air mass backward trajectories were calculated using the HYSPLIT Model (http://ready.arl.noaa.gov/HYSPLIT.php).

$PM_{2.5}$ were collected onto the Whatman quartz fiber filters for 12 h starting from 7:00 a.m. or 7:00 PM, by a high-volume air sampler (XT1025, Shanghai XTtust Analytical Instruments Co., LTD) at a flow rate of 1.00 m^3/min. All the filters were pre-baked at

470 °C to remove organic matter. Before and after the collection, the filters were weighed under the constant temperature and humidity. The $PM_{2.5}$-loaded filters were wrapped in aluminum foil and stored in a refrigerator at −18 °C until chemical analysis. The sampling was not continuous in this work, and a total of 40 daytime samples and 39 nighttime samples were effectively obtained (Fig. S1 showed the effective sampling information.). Each $PM_{2.5}$-loaded filter was punched into several pieces of different areas (three pieces of 6 cm^2, three pieces of 30 cm^2, one piece of 10 cm^2, one piece of 12 cm^2 and other pieces not for this work) for chemical analyzing and ROS-generation measurement.

A piece of 6 cm^2 of $PM_{2.5}$-loaded filter was first submerged in a vial with 10 mL ultrapure water. After 30 min of ultrasonic extraction, the solution was filtrated through a Teflon filter (0.45 mm), and then analyzed by ion chromatography (Dionex ICS-3000). This procedure measured the water soluble inorganic ions, including three anions (SO_4^{2-}, NO_3^-, Cl^-) and five cations (NH_4^+, K^+, Ca^{2+}, Na^+ Mg^{2+}).

Another piece of 6 cm^2 was put in a digestion tank to undergo the digesting by a mixture of 4.5 mL HNO_3, 1.5 mL HCl and 1.5 mL HF at 190 °C for 40 min. After cooling to room temperature, the solution was diluted to 20 mL with ultrapure water. Six typical transition metals (Fe, Cu, Mn, V, Co, Ni) that were usually regarded as capable to generate ROS were analyzed by an inductively coupled plasma-mass spectrometer (ICP-MS, Thermo Fisher ICAP RQ).

The 10 cm^2 piece was used for carbonaceous species analysis. After 40 min ultrasonic extraction, the solution was filtered with a PTFE filter (0.45 μm). Using a TOC analyzer (multi N/C UV HS, Analytik Jena AG, Germany) and a thermal/optical carbon analyzer (DRI Model, 2001A, USA), we measured the WSOC, EC and OC concentrations for each 12-h $PM_{2.5}$ sample. The detection limit for the TOC analyzer was 2 μg/L, and in this study the raw data we measured were all at the mg/L level. Besides, water-insoluble organic compounds (WISOC) concentrations were obtained by subtracting WSOC concentrations from the total OC concentrations.

The 12 cm^2 piece was used for the Gas Chromatography-tandem Mass Spectrometry (GC-MS/MS) quantification of quinones contained in $PM_{2.5}$. The pretreatment protocol are as described in Delgado-Saborit et al. (2013). The filter was extracted three times in dichloromethane for 30 min. The volumes of dichloromethane were 3 mL, 2 mL and 1 mL, respectively. The total extract was filtered by PTFE membrane (0.45 μm), eluted by 1 mL of dichloromethane, and blown-dry by nitrogen. Then, 100 mg zinc powder and 200 μL acetic anhydride were mixed with the extract to help change the quinones to their diacetyl derivatives. The mixture was shaken and heated at 80 °C for 15 min. After cooling, dilution and centrifugation, the upper organic layer (about 3 mL) was blown by nitrogen, and finally diluted in the 100 μL dichloroethane for GC-MS/MS analysis (Agilent Technologies Inc., Wilmington, DE). In this work, 7 quinones were measured, including 1,4-naphthoquinone, 1,2-naphthoquinone, 2-hydroxyl-1,4-naphthoquinone, 5-hydroxyl-1,4-naphthoquinone, 9,10-phenanthraquinone, 9,10-anthraquinone and benz(a)anthracene-7,12-quinone. After each of the 7 quinones was quantified, we calculated the naphthoquinone mass equivalent (which converts the measured mass of every quinones to the mass of naphthoquinone with the same moles of conjugated cyclic dione structure), then the total quinones concentrations were obtained.

A 30 cm^2 piece was used for HULIS species analysis (Lin et al., 2010). The piece was submerged in a vial with 25 mL ultrapure water. After the 40-min ultrasonic water-bath, the extract was acidified with 2.4 M HCl until the pH value was 2, and then was eluted through the SPE cartridge (Oasis HLB, 30 μm, 60 mg/cartridge, Waters, USA). Notice that the SPE cartridge was in advance rinsed with 2 mL ultrapure water in order to remove the remaining soluble matter from the cartridge. Since the HULIS were retained on the SPE cartridge, 12 mL methanol was added to the column (3 mL × 4 times), and the extracted organic matter was blown by nitrogen and dried to a yellow stain. The obtained HULIS sample was then dissolved in 20 mL water, and measured by the TOC analyzer. Since the TOC analysis only measures the amount of carbon in the analyzed organic sample, the HULIS concentration was in the unit of μgC/m^3.

In addition, the light absorption spectra of the HULIS sample (obtained by the same method as above from a 30 cm^2 piece) were measured by UV−vis spectrophotometer (J&M Analitik AG, Germany). After that, the mass absorption efficiency (MAE, unit: m^2/g), which represents the light absorbance per unit mass of HULIS, was estimated using equation (1).

$$MAE_\lambda = (A_\lambda - A_{700}) \times \frac{V_w}{V \times L \times C} \times \ln(10) \quad (1)$$

λ (nm) is the wavelength, V_w (mL) is the extraction volume of HULIS, and V (m^3) represents the volume of air sampled during the sampling. L (cm) is the path length of light, and C (μgC/m^3) refers to the concentration of HULIS.

2.2. Measurement of the ·OH generation in SLF

In this work, we used the ·OH measurement in SLF to characterize the ROS-generation potential. The measurement was applied to both the $PM_{2.5}$ and the HULIS, but the pretreatment was a little different.

For the measurement for HULIS, the HULIS isolated from a piece of 30 cm^2 of $PM_{2.5}$-loaded filter was dissolved into a 20 mL HULIS aqueous solution, just as described in the above section about HULIS concentration measurement. A bulk of phosphate-buffered saline (PBS) was prepared meanwhile. The pH value of the PBS was buffered in the range of 7.2−7.4 using 114 mM NaCl, 7.8 mM Na_2HPO_4 and 2.2 mM KH_2PO_4. Both the HULIS aqueous solution and PBS were pre-treated with a Chelex-100 resin column to remove the trace metals. After that, antioxidants and the ·OH chemical probe were dissolved in the PBS to make a SLF solution, and then 3.2 mL HULIS aqueous solution was added into 2.8 mL SLF solution to form a 6 mL reaction mixture for ·OH generation. In this work, we used L-ascorbic acid (Asc), citric acid (Cit), L-glutathione (GSH) and uric acid (UA) as antioxidants, and we used disodium terephthalate (TPT) as the ·OH chemical probe. Their initial concentrations in the 6 mL reaction solution were 200 μM Asc, 300 μM Cit, 100 μM GSH, 100 μM UA and 12 mM TPT. In addition, as a blank control sample, a piece of 30 cm^2 of unloaded filter was used to undergo the same process.

For the measurement for $PM_{2.5}$, a piece of 6 cm^2 of $PM_{2.5}$-loaded filter was sonicated in 3.2 mL water with 50 μL 2,2,2-trifluoroethanol for 40 min. The SLF solution was as prepared as above. After the sonication 3.2 mL solution as well as the $PM_{2.5}$-loaded filter were both mixed with 2.8 mL SLF solution to mimic the endogenous radical generation. Also, we used a piece of 6 cm^2 of unloaded filter as a blank control sample.

The reaction mixture, for whether HULIS or $PM_{2.5}$, was shaken and kept in a 37 °C water bath for 4 h. During the 4-h reaction, ·OH could be produced from the $PM_{2.5}$ or HULIS. Since TPT in the solution traps ·OH to generate 2-hydroxyterephtalic acid (OHTA), ·OH production can be quantified by measuring the OHTA concentration. We draw a 1 mL aliquot of the reaction mixture and shook the remaining mixture every 30 min. The drawn mixture was mixed immediately with 0.5 mL of 100 mM dimethyl sulfoxide (aq) to quench the ·OH production. The OHTA concentration ([OHTA] in M) in the mixture was measured by a spectrofluorometer (Horiba

Fluoromax-4L) at excitation/emission wavelengths of 315/430 nm. OHTA was measured three times and the mean value of the results was taken as the final [OHTA]. The ·OH concentration ([·OH] in M) was then calculated after dividing the measured [OHTA] by 0.35 (the molar yield of OHTA produced from the reaction of ·OH with TPT at pH 7.2–7.4 in SLF) (Li et al., 2019a). Therefore, the ·OH production rate ($R_{\cdot OH}$ in ng/h) for each sample was obtained by fitting [·OH] after different reaction time and integrating the 6 mL (the volume of the reaction mixture). We conducted blank control correction by deducting the ·OH generation rate for the blank control sample ($R^0_{\cdot OH}$ in ng/h) to gain the corrected ·OH generation rate ($R^*_{\cdot OH}$ in ng/h). The $R^*_{\cdot OH}$ was finally normalized by the mass of $PM_{2.5}$ or HULIS, by using equations (2) and (3). To keep the abbreviation consistency with other relevant literature (Bates et al., 2019; Yu et al., 2020), we termed the normalized $R^*_{\cdot OH}$ as OP^{OH-SLF} (which is the abbreviation of the oxidative potential obtained by the ·OH measurement in SLF). It was then prefixed to be PM-OP^{OH-SLF} (unit: ng/h/μg$PM_{2.5}$) and HULIS-OP^{OH-SLF} (unit: ng/h/μgC) for the $PM_{2.5}$ and HULIS, respectively.

$$PM-OP^{OH-SLF} = \frac{R^*_{\cdot OH} \text{ for } PM_{2.5} \text{ piece}}{PM_{2.5} \text{ mass in filter} \times \text{piece area/filter area}} \quad (2)$$

$$HULIS-OP^{OH-SLF} = \frac{R^*_{\cdot OH} \text{ for the isolated HULIS sample}}{\text{isolated HULIS mass in the piece}} \quad (3)$$

The ROS-generation potential by $PM_{2.5}$ can also be normalized to air volume using equation (4), which we refer to as PM-OP_v^{OH-SLF} (unit: ng/h/m^3) in this manuscript.

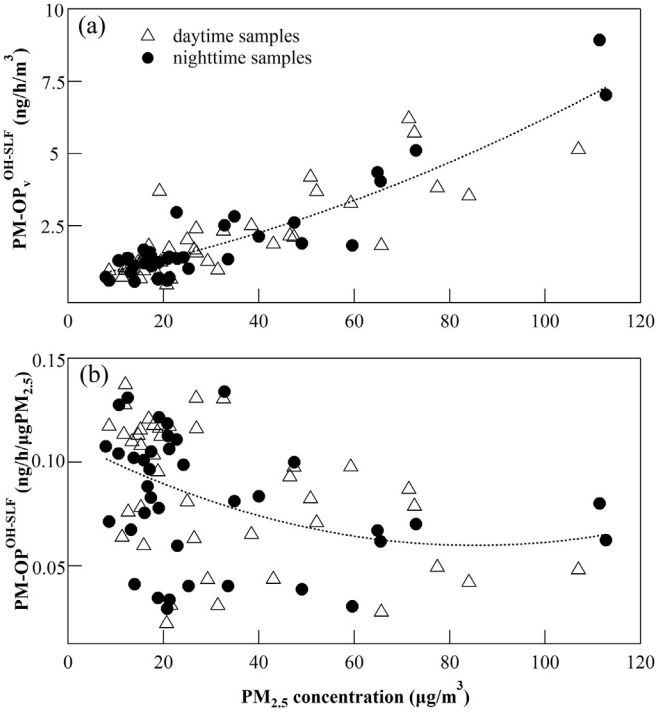

Fig. 1. (a) Comparison between the PM-OP_v^{OH-SLF} and the ambient $PM_{2.5}$ concentration; (b) Comparison between the PM-OP^{OH-SLF} and the ambient $PM_{2.5}$ concentration. The daytime samples and nighttime samples were labelled as hollow triangles and solid circles respectively.

$$PM-OPv^{OH-SLF} = \frac{R^*_{\cdot OH} \text{ for } PM_{2.5} \text{ piece}}{PM_{2.5} \text{ sampling flow rate} \times \text{sampling time} \times \text{piece area/filter area}} \quad (4)$$

3. Results and discussion

3.1. PM-OP^{OH-SLF} slightly decreased with the rise of $PM_{2.5}$ concentration

Aerosol particles are of higher concentration in the polluted days so that the ROS production per unit volume of air is enhanced. We also found this to be the case in our measurements where PM-OP_v^{OH-SLF} increased as $PM_{2.5}$ concentration increased, as shown in Fig. 1(a). However, the different chemical reactivity of various chemicals indicates that aerosols possibly differ among different components in their oxidative potential. Hence, it is better to use the mass-normalized PM-OP^{OH-SLF} rather than PM-OP_v^{OH-SLF} to characterize the aerosol toxicity. A recent study in the North China Plain have revealed the lower radical production per unit mass of $PM_{2.5}$ on more polluted days (Li et al., 2019a). Similar phenomenon was observed in our field measurement work in urban Shanghai. As shown in Fig. 1(b), samples with higher PM-OP^{OH-SLF} occurred when $PM_{2.5}$ concentrations were lower. Besides, the daytime samples and nighttime samples were evenly distributed in Fig. 1. They showed similar relationship between PM-OP_v^{OH-SLF} or PM-OP^{OH-SLF} and $PM_{2.5}$ concentration, indicating no apparent diurnal variation for the ROS-generation potential of $PM_{2.5}$.

The mild decrease of ROS production with the rise of $PM_{2.5}$ concentration in the North China Plain was attributed to the increased percentage of SNA (sulfates, nitrates and ammoniums, which are the major water soluble inorganic ions but hardly contributed to the oxidative potential) in high $PM_{2.5}$ concentration events (Li et al., 2019a). The similar reason goes for our observation in this study. As shown in Fig. 2, the mass proportions of OC and WSOC in $PM_{2.5}$ both presented a decreasing trend when $PM_{2.5}$ concentration was increasing, though their volume concentration still increased. The transition metals measured in this work contained Fe, Cu, Mn, V, Co and Ni, most of which have been reported as typical ROS-generating species (Charrier and Anastasio, 2011, 2012; 2015; Verma et al., 2010). Fig. 2(c) for the total concentration of the measured metals showed a scattered pattern more than an increasing trend. It could be due to the major proportion of Fe among the measured metals. As shown in Fig. S2, the increasing trends of the volume concentrations of Mn and Cu were even more apparent than that of Fe. Though, the decrease of mass ratio with the rise of $PM_{2.5}$ was commonly observed for all the measured metals. Contrary to the organics and transition metals, SNA concentration per unit mass of $PM_{2.5}$ almost kept stable under a wider range of $PM_{2.5}$ concentrations in this work, as shown in Fig. 2(h). The average mass proportion of SNA in $PM_{2.5}$ was higher than organics and metals, indicating $PM_{2.5}$ was dominated by SNA in urban Shanghai atmosphere. We can also infer that some insoluble components like mineral dust increased with the $PM_{2.5}$ concentration increasing, and these components as well as SNA hardly

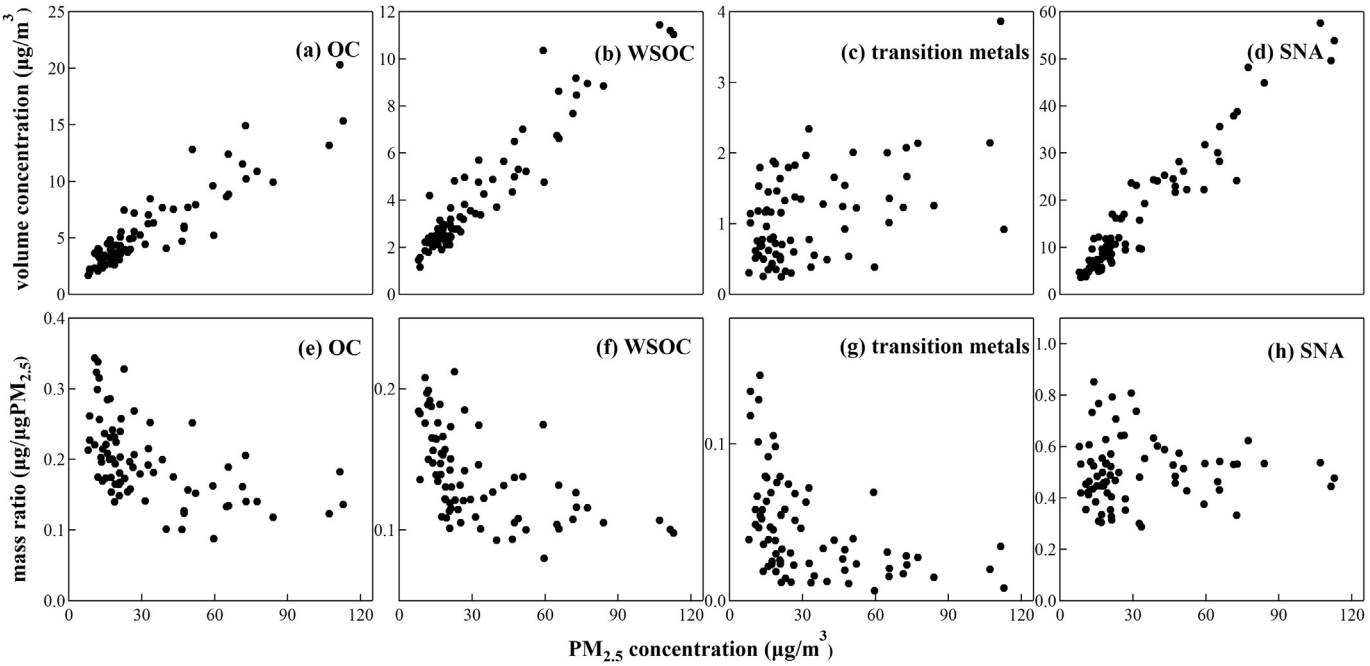

Fig. 2. Correlation scatter plots of (a&e) the OC concentrations, (b&f) WSOC concentrations, (c&g) total concentration of the measured typical transition metals and (d&h) SNA concentration versus the $PM_{2.5}$ concentration. The concentrations of the four species were in per unit volume of air for (a–d), but in per unit mass of $PM_{2.5}$ for (e–h).

contributed to the ROS-generation potential of aerosols.

3.2. Correlation between PM-$OP^{OH\text{-}SLF}$ and different components in $PM_{2.5}$

The above discussion about the PM-$OP^{OH\text{-}SLF}$ and fractional concentrations of different components showed that both organics and typical transition metals were important contributors to the ROS-generation potential. First, correlation of PM-$OP^{OH\text{-}SLF}$ with different metals was investigated, with the correlation plots illustrated in Fig. S3. Among the six metals we measured, Fe accounted for the majority not only in mass but also in the correlation with PM-$OP^{OH\text{-}SLF}$. It accords with the critical ability of Fe to produce ·OH by Fenton-like reactions (Charrier and Anastasio, 2011; Pang et al., 2019). In addition to Fe, V was found to be also well-related with PM-$OP^{OH\text{-}SLF}$, even better than Cu. It implies the possible role by ship related aerosols in health effects (Zhang et al., 2019). Moreover, it should be noticed that the metal concentrations here were the total concentrations of the metals with different solubility. Though water-soluble metals were generally considered to be strongly associated with the ROS-generation, some reports have taken more attention to the ROS-generation potential by the insoluble aerosol species, including the insoluble transition metals (McWhinney et al., 2013; Fang et al., 2017).

According to the water-solubility, OC can be classified into WSOC and WISOC. Fig. 3(a–c) illustrated the Pearson correlation analysis conducted among PM-$OP^{OH\text{-}SLF}$ and the OC with different water-solubility. Apparently, WSOC presented stronger positive correlation ($R = 0.62$) with PM-$OP^{OH\text{-}SLF}$ than WISOC did. This observation is in agreement with findings by DTT assays (Verma et al., 2012) that water-solubility helped enhance the ROS-generation potential of the organics. WSOC, however, represents a complex mixture of a number of organics. HULIS are special organics chromatographically isolated from WSOC. In this work, HULIS were highly positively correlated with the $PM_{2.5}$ in concentration (Fig. 3 (f)), and they accounted for 57 ± 16% of WSOC. This ratio was consistent with the reported ratio of HULIS in WSOC in urban Shanghai annually (Zhao et al., 2016). As shown in Fig. 3 (d), HULIS presented a so strong correlation with PM-$OP^{OH\text{-}SLF}$ as WSOC did. In addition, despite quinones as the surrogates of ROS-generating OC (Lyu et al., 2018), the correlation of HULIS with ROS_{PM} was even stronger than that of quinones in this work. Therefore, isolated HULIS samples were in detail investigated in the following section.

3.3. ROS-generation by HULIS in $PM_{2.5}$

Given the importance of HULIS in $PM_{2.5}$, we isolated the HULIS species from the collected samples. Comparing to the PM-$OP^{OH\text{-}SLF}$ which presented the integrated effects on the oxidative potential by all kinds of aerosol components, HULIS-$OP^{OH\text{-}SLF}$ here was to characterize the ·OH generated by HULIS. Though trace amount of other species could still be retained, the influence of the complicated interactions between HULIS and other particulate species should be lowered greatly enough to study the ROS-generation potential by HULIS species alone.

For the 79 samples of this work, the HULIS concentration ranged from 0.55 μg C/m^3 to 5.90 μg C/m^3 with the average of 2.29 μg C/m^3, while the HULIS-$OP^{OH\text{-}SLF}$ ranged from 0.026 ng/h/μgC to 0.302 ng/h/μgC with the average of 0.112 ng/h/μgC. We plotted the HULIS-$OP^{OH\text{-}SLF}$ versus HULIS concentration in Fig. 4, and found that the samples with above-average HULIS-$OP^{OH\text{-}SLF}$ were mostly of below-average HULIS concentration. This observation indicated that HULIS during the less polluted periods could also have strong ROS-generation potential. For convenience, the HULIS with above-average HULIS-$OP^{OH\text{-}SLF}$ and below-average HULIS concentration, which corresponds to the icons in the top-left part of Fig. 4 (a) or (b), were abbreviated as High-ROS/Low-Conc HULIS in the following discussion.

Some laboratory studies have demonstrated that SOA formed via different reaction pathways have different ROS-generation potential, implying the ROS-generation potential of the organic

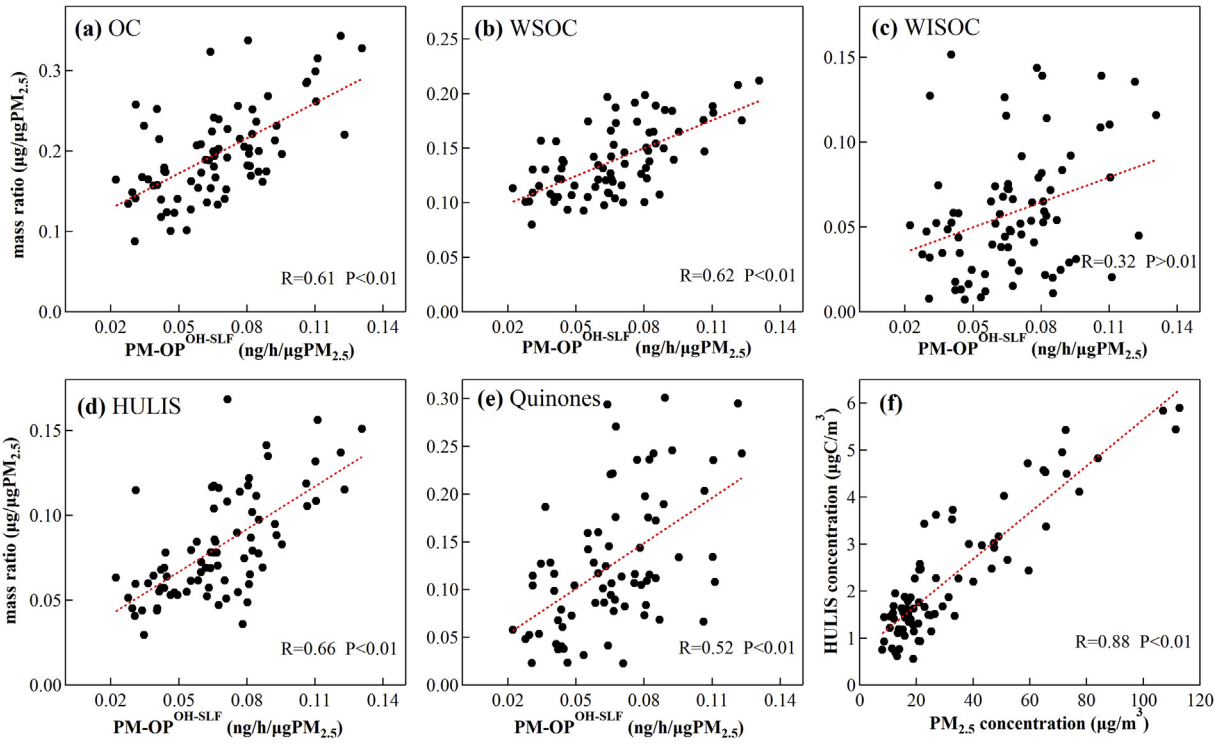

Fig. 3. Correlation scatter plots of (a) the OC/$PM_{2.5}$ mass ratio, (b) WSOC/$PM_{2.5}$ mass ratio, (c) WISOC/$PM_{2.5}$ mass ratio, (d) HULIS/$PM_{2.5}$ mass ratio and (e) Quinones/$PM_{2.5}$ mass ratio versus the PM-$OP^{OH\text{-}SLF}$. Here the Quinones mass is the sum of mass of 7 quinones we measured in this work. (f) Correlation between HULIS concentration and $PM_{2.5}$ concentration.

compounds usually depends on their molecular structure (Jiang et al., 2016; Kramer et al., 2016). Thus, the special HULIS-$OP^{OH\text{-}SLF}$ distribution over HULIS concentration indicated that the HULIS with higher ROS-generation potential could differ in the chemical structure from the other HULIS. Molecular difference among HULIS species could results from different sources and atmospheric secondary processes (Tan et al., 2016; Win et al., 2018). Biomass burning emitted HULIS were generally considered as the main ROS-generating HULIS (Wang et al., 2017; Ma et al., 2018, 2019). In this study, pollution events caused by biomass burning were identified by air mass back trajectories and the fire spot maps. During our sampling periods, there was only one typical biomass burning event with effective sampling (between December 16 and December 19, 2018). The corresponding fire spot maps integrated with air mass back trajectories for the days (Fig. S4) showed that biomass burning particles could be transported from the inland areas to Shanghai during December 16–19. Correspondingly, $PM_{2.5}$ and HULIS concentrations were apparently higher than the days before and after the event (Fig. S5). A good correlation ($R = 0.97$) between water soluble K^+ concentration (a typical marker for biomass burning emission) and $PM_{2.5}$ concentration confirmed that the pollution event was mainly caused by biomass burning. Yet it surprised us that the HULIS-$OP^{OH\text{-}SLF}$ in this event were comparatively low, as shown in Fig. S5 and labelled in Fig. 4(a). None of the samples in the biomass burning influenced event belonged to High-ROS/Low-Conc HULIS, implying that High-ROS/Low-Conc HULIS we observed in this work cannot be ascribed to biomass burning emission. In other words, secondary process could contribute more to these special HULIS.

The atmospheric secondary process usually includes oxidation, oligomerization, reduction and fragmentation for atmospheric organic compounds (Yu et al., 2014). Oxidation is regarded as the most principal chemical process. During our effective sampling dates, the ambient 12-h average O_3 concentration ranged from 4.5 μg/m^3 to 164.6 μg/m^3 with the average of 54.8 μg/m^3. However, the O_3 concentrations were not positively related with the ROS-generation of HULIS in our observation. As shown in Fig. 4(b), the above-average HULIS-$OP^{OH\text{-}SLF}$ were largely observed when the ambient 12-h average O_3 concentrations were below 54.8 μg/m^3. This observation suggested that the occurrence of High-ROS/Low-Conc HULIS in this study was likely not related to the atmospheric oxidation process. On the other hand, HULIS samples collected on the high O_3 concentration days had moderate HULIS concentrations and low HULIS-$OP^{OH\text{-}SLF}$. Though the known chemicals with high ROS-generation potential contains secondary organics formed via atmospheric oxidation reaction (McWhinney et al., 2013; Tuet et al., 2017), further oxidation in the real atmosphere would lead to such SOA derivatives as organosulfates. Organosulfate derivatives were reported to be hardly contributing in ROS-generation (Kramer et al., 2016).

The ratios of nighttime samples to daytime samples were calculated for the four regions in Fig. 4 separated by the average lines. They are 1.67, 0.81, 0.67 and 0.70 for the top-left, bottom-left, top-right and bottom-right respectively. The apparent higher ratio for the top-left implied that High-ROS/Low-Conc HULIS tended to form in dark environment. We further checked the relative humidity variation during our experiment. Since the samples were collected every 12 h while the RH value was hourly resolved, each sample had 12 corresponding RH values. We compared the RH distribution for High-ROS/Low-Conc HULIS with that for other HULIS. As shown in Fig. S6, High-ROS/Low-Conc HULIS tended to occur at higher RH condition. The observations about the daytime/nighttime sample ratio and the RH distribution suggested that photochemical reactions were not the pivotal process to the formation of High-ROS/Low-Conc HULIS in this work, while atmospheric aqueous-phase reactions might be important contributors to their formation. Aqueous-phase reactions are the typical secondary processes for aerosols under high humidity and during

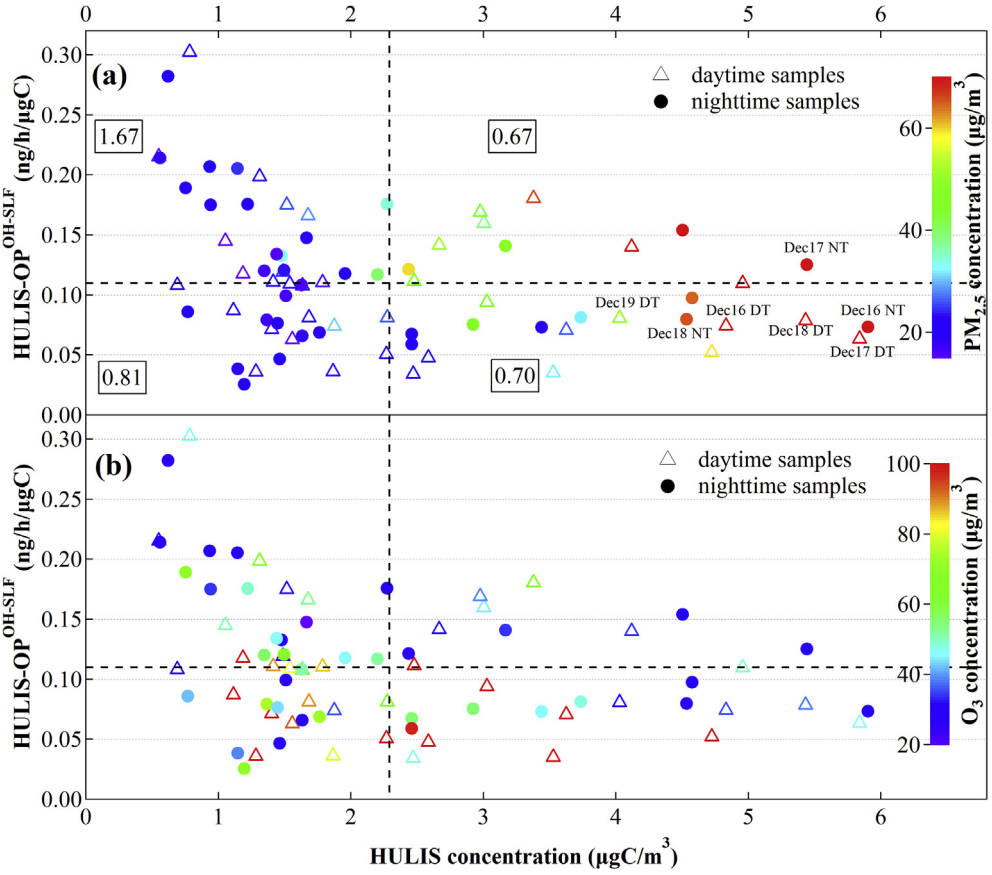

Fig. 4. HULIS-$OP^{OH\text{-}SLF}$ (ng/h/μgC) were plotted versus HULIS concentration (μgC/m^3). The dash lines paralleled to x and y axes presented the average values of HULIS-$OP^{OH\text{-}SLF}$ and HULIS concentration respectively. The daytime samples and nighttime samples were labelled as hollow triangles and solid circles respectively. (a) and (b) are the same plot except that the icons were colored in $PM_{2.5}$ concentration in (a) and colored in O_3 concentration in (b). The box framed numbers with two decimal places in (a) were the ratios of nighttime samples to daytime samples in the four regions separated by the dash lines. Besides, the samples corresponding to the biomass burning event during December 16 to 19 were labelled with time information in (a).

nights (Sun et al., 2013). The typical aqueous-phase reactions in the atmosphere include oligomerization like aldol condensation and reduction such as carbonyl-to-imine reaction. Recent researches on SOA formation, including ours, demonstrated that the atmospheric aqueous-phase reactions could lead to the formation of nitro-compounds or heterocyclic compounds (Laskin et al., 2015; Li et al., 2019b; Pang et al., 2019). These N-containing SOA could promote electron transfer to enhance the oxidative potential.

The above discussion suggests that the High-ROS/Low-Conc HULIS might mainly come from nocturnal chemistry. However, not all HULIS formed via nocturnal reaction would have high ROS-generation potential. Nighttime HULIS could contain other kinds of organics (e.g. organosulfates, organonitrates, CHO polymers), which could be the main components for nighttime HULIS in the bottom-left region of Fig. 4.

3.4. Light-absorbance of HULIS with different ROS-generation potential

The above discussion demonstrated that HULIS species, though they were usually regarded as a type of compounds with similar chemical characteristics, exhibited different ROS-generation potential. To further understand these High-ROS/Low-Conc HULIS, we analyzed the MAE for the isolated HULIS species and compared the light-absorption by High-ROS/Low-Conc HULIS with that by the other HULIS. As shown in Fig. 5, the HULIS species have strong absorbance at the wavelengths below 600 nm. It is consistent with the reported knowledge that HULIS are a sort of light-absorbing compounds in aerosols (also known as Brown Carbon) because of their high molecular-weight and conjugated structures (Laskin et al., 2015). High-ROS/Low-Conc HULIS showed a stronger absorbability in average for the entire UV–visible wavelength than the other HULIS. We also noticed that MAE at wavelengths below 350 nm varied more widely for High-ROS/Low-Conc HULIS than for the other HULIS. Because the near-ultraviolet absorbance results from the electronic transitions of organic functional groups, the large variation of MAE indicated that High-ROS/Low-Conc HULIS contained many different types of functional groups resulted from secondary reactions. In-depth molecular-level characterization should be carried out in the future studies to uncover their molecular structures. In addition, since the HULIS with stronger ROS-generation potential and light-absorbance were mainly detected when the $PM_{2.5}$ concentrations were low, this work illuminates the importance for HULIS species during less polluted or even clean periods.

3.5. Atmospheric implications

HULIS is an important part of atmospheric organic aerosols. Combustions like biomass burning and atmospheric secondary processes are the main sources of HULIS (Zheng et al., 2013). Many previous studies on HULIS have highlighted the biomass burning emitted HULIS as the major contributor to the ROS-generation (Wang et al., 2017; Ma et al., 2018, 2019). However, in this work,

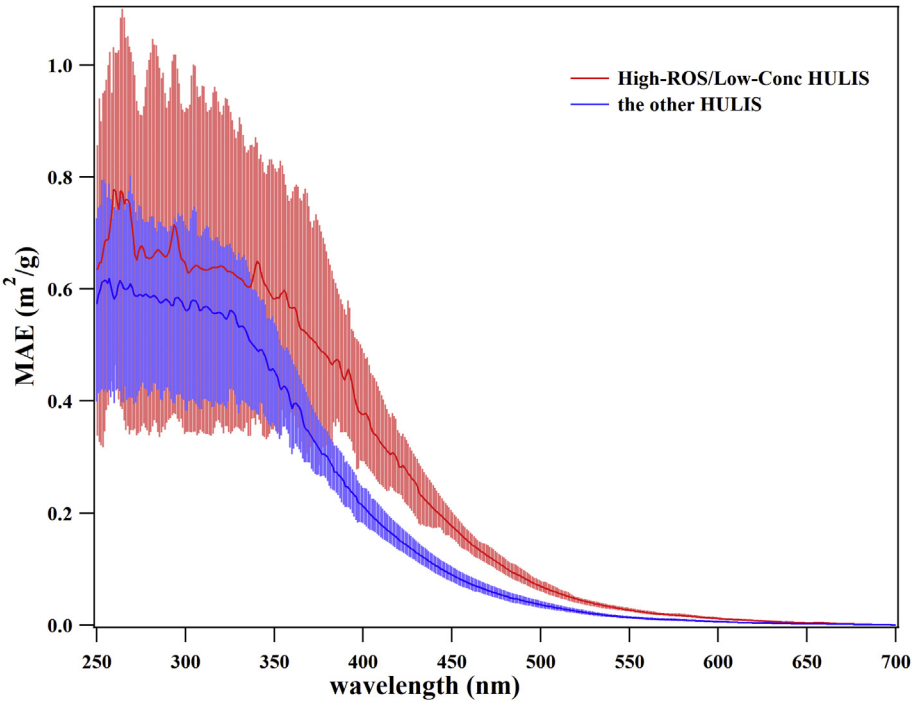

Fig. 5. Integrated MAE of High-ROS/Low-Conc HULIS and the other HULIS observed in our work. The average MAE for the two HULIS species were full-lined.

by assessing the mass-normalized ·OH production by HULIS, we found in urban Shanghai that HULIS presented during low $PM_{2.5}$ pollution periods were more capable to produce ROS. These special HULIS with high ROS-generation potential were neither related to the biomass burning influence event, nor well correlated to the O_3 concentration. They were possibly the products of atmospheric aqueous-phase reactions such as oligomerization or reduction. The results indicated that some of the HULIS species in the non-hazy days were more toxic in terms of their intrinsic radical production capability. It underlined the materiality of the urban organic aerosols, no matter whether the $PM_{2.5}$ concentration was high or low. Assessment on the adverse health effects by aerosols should address the chemical compositions of the aerosols, instead of only focusing on the mass concentration.

High-ROS/Low-Conc HULIS observed in this work were also found to have stronger light-absorbance than the other HULIS, implying that these special HULIS may play important roles in determining aerosol's radiative forcing. Also, the HULIS with high ROS-generation potential may act as photosensitizers to enhance atmospheric photochemical reactions. Therefore, even if the total $PM_{2.5}$ concentration is not high in urban atmosphere, the organic components including HULIS are unneglectable when evaluating aerosols' influence upon human health, solar radiation, visibility and atmospheric evolution.

Moreover, the observation of High-ROS/Low-Conc HULIS in this work does not mean the absence of these special HULIS species when $PM_{2.5}$ concentration is high. Similar HULIS species could also be formed during highly-polluted days, but their ·OH production or light absorbance might be covered by the high-concentration HULIS from other primary or secondary sources.

4. Conclusion

In this work, we collected $PM_{2.5}$ samples in the urban atmosphere of Shanghai during autumn and winter (2018–2019), and assessed the ROS-generation potential of $PM_{2.5}$ and of the isolated HULIS species by measuring the ·OH production rate in SLF. The measured ROS-generation potential of $PM_{2.5}$ decreased with the increase of $PM_{2.5}$ concentration, mainly due to the high ratio of inorganic components in the increased $PM_{2.5}$. The correlation studies between the mass concentration and the oxidative potential showed that HULIS were the major organic components contributing to the ROS-generation potential of $PM_{2.5}$. We investigated the ·OH production by the isolated HULIS as well. The special HULIS with high HULIS-$OP^{OH\text{-}SLF}$ were observed when the $PM_{2.5}$ concentration and HULIS concentration were relatively low. These High-ROS/Low-Conc HULIS had no relation with the biomass burning pollution event in our work. They were likely formed through aqueous-phase reactions especially during nighttime or under high relative humidity conditions. Optical property analysis indicated that High-ROS/Low-Conc HULIS were more light-absorbing than the other HULIS. Our results implied that HULIS might play important roles in terms of aerosol's health effect, solar radiative balance and atmospheric processes even when the $PM_{2.5}$ pollution is low. In future, in-depth molecular characterization should be carried out to have a better understanding of these special HULIS.

Declaration of competing interest

The authors declare that they have no known competing financial interests or personal relationships that could have appeared to influence the work reported in this paper.

CRediT authorship contribution statement

Xiaoya Xu: Investigation, Writing - original draft. **Xiang Li:** Conceptualization, Validation, Writing - review & editing, Methodology. **Yaxi Liu:** Visualization. **Xiaofei Wang:** Methodology. **Hong Chen:** Data curation. **Jianmin Chen:** Resources. **Xin Yang:** Conceptualization, Supervision, Project administration. **Tzung-May Fu:** Writing - review & editing. **Qianbiao Zhao:** Investigation.

Qingyan Fu: Resources.

Acknowledgments

This work was supported by the National Natural Science Foundation of China (Nos. 41775150, 21976034 and 41827804).

Appendix A. Supplementary data

Supplementary data to this article can be found online at https://doi.org/10.1016/j.chemosphere.2020.127050.

References

Bates, J.T., Fang, T., Verma, V., Zeng, L., Weber, R.J., Tolbert, P.E., Abrams, J.Y., Sarnat, S.E., Klein, M., Mulholland, J.A., Russell, A.G., 2019. Review of acellular assays of ambient particulate matter oxidative potential: methods and relationships with composition, sources, and health effects. Environ. Sci. Technol. 53, 4003–4019.

Brook, R.D., Rajagopalan, S., Pope, C.A., Brook, J.R., Bhatnagar, A., Diez-Roux, A.V., Holguin, F., Hong, Y., Luepker, R.V., Mittleman, M.A., Peters, A., Siscovick, D., Smith Jr., S.C., Whitsel, L., Kaufman, J.D., 2010. Particulate matter air pollution and cardiovascular disease an update to the scientific statement from the American heart association. Circulation 121, 2331–2378.

Charrier, J.G., Anastasio, C., 2011. Impacts of antioxidants on hydroxyl radical production from individual and mixed transition metals in a surrogate lung fluid. Atmos. Environ. 45, 7555–7562.

Charrier, J.G., Anastasio, C., 2012. On dithiothreitol (DTT) as a measure of oxidative potential for ambient particles: evidence for the importance of soluble transition metals. Atmos. Chem. Phys. 12, 9321–9333.

Charrier, J.G., Anastasio, C., 2015. Rates of hydroxyl radical production from transition metals and quinones in a surrogate lung fluid. Environ. Sci. Technol. 49, 9317–9325.

Charrier, J.G., McFall, A.S., Richards-Henderson, N.K., Anastasio, C., 2014. Hydrogen peroxide formation in a surrogate lung fluid by transition metals and quinones present in particulate matter. Environ. Sci. Technol. 48, 7010–7017.

Charrier, J.G., Richards-Henderson, N.K., Bein, K.J., McFall, A.S., Wexler, A.S., Anastasio, C., 2015. Oxidant production from source-oriented particulate matter-Part 1: oxidative potential using the dithiothreitol (DTT) assay. Atmos. Chem. Phys. 15, 2327–2340.

Chen, Q., Ikemori, F., Higo, H., Asakawa, D., Mochida, M., 2016. Chemical structural characteristics of HULIS and other fractionated organic matter in urban aerosols: results from mass spectral and FT-IR analysis. Environ. Sci. Technol. 50, 1721–1730.

Chen, Q., Wang, M., Wang, Y., Zhang, L., Li, Y., Han, Y., 2019. Oxidative potential of water-soluble matter associated with chromophoric substances in $PM_{2.5}$ over xi'an, China. Environ. Sci. Technol. 53, 8574–8584.

Cho, A.K., Sioutas, C., Miguel, A.H., Kumagai, Y., Schmitz, D.A., Singh, M., Eiguren-Fernandez, A., Froines, J.R., 2005. Redox activity of airborne particulate matter at different sites in the Los Angeles Basin. Environ. Res. 99, 40–47.

Delfino, R.J., Sioutas, C., Malik, S., 2005. Potential role of ultrafine particles in associations between airborne particle mass and cardiovascular health. Environ. Health Perspect. 113, 934–946.

Delgado-Saborit, J.M., Alam, M.S., Godri Pollitt, K.J., Stark, C., Harrison, R.M., 2013. Analysis of atmospheric concentrations of quinones and polycyclic aromatic hydrocarbons in vapour and particulate phases. Atmos. Environ. 77, 974–982.

Dou, J., Lin, P., Kuang, B.-Y., Yu, J.Z., 2015. Reactive oxygen species production mediated by humic-like substances in atmospheric aerosols: enhancement effects by pyridine, imidazole, and their derivatives. Environ. Sci. Technol. 49, 6457–6465.

Fan, X., Song, J., Peng, P.a., 2016. Temporal variations of the abundance and optical properties of water soluble Humic-Like Substances (HULIS) in $PM_{2.5}$ at Guangzhou, China. Atmos. Res. 172, 8–15.

Fang, T., Zeng, L., Gao, D., Verma, V., Stefaniak, A.B., Weber, R.J., 2017. Ambient size distributions and lung deposition of aerosol dithiothreitol-measured oxidative potential: contrast between soluble and insoluble particles. Environ. Sci. Technol. 51, 6802–6811.

Godri, K.J., Harrison, R.M., Evans, T., Baker, T., Dunster, C., Mudway, I.S., Kelly, F.J., 2011. Increased oxidative burden associated with traffic component of ambient particulate matter at roadside and urban background schools sites in London. PloS One 6, e21961.

Gonzalez, D.H., Cala, C.K., Peng, Q., Paulson, S.E., 2017. HULIS enhancement of hydroxyl radical formation from Fe(II): kinetics of fulvic acid-Fe(II) complexes in the presence of lung antioxidants. Environ. Sci. Technol. 51, 7676–7685.

Hedayat, F., Stevanovic, S., Miljevic, B., Bottle, S., Ristovski, Z.D., 2015. Review - evaluating the molecular assays for measuring the oxidative potential of particulate matter. Chem. Ind. Chem. Eng. Q. 21, 201–210.

Huang, R.J., Cheng, R., Jing, M., Yang, L., Li, Y., Chen, Q., Chen, Y., Yan, J., Lin, C., Wu, Y., Zhang, R., El Haddad, I., Prevot, A.S.H., O'Dowd, C.D., Cao, J., 2018. Source-specific health risk analysis on particulate trace elements: coal combustion and traffic emission as major contributors in wintertime beijing. Environ. Sci. Technol. 52, 10967–10974.

Ito, K., Mathes, R., Ross, Z., Nadas, A., Thurston, G., Matte, T., 2011. Fine particulate matter constituents associated with cardiovascular hospitalizations and mortality in New York City. Environ. Health Perspect. 119, 467–473.

Jiang, H.H., Jang, M., Sabo-Attwood, T., Robinson, S.E., 2016. Oxidative potential of secondary organic aerosols produced from photooxidation of different hydrocarbons using outdoor chamber under ambient sunlight. Atmos. Environ. 131, 382–389.

Kramer, A.J., Rattanavaraha, W., Zhang, Z., Gold, A., Surratt, J.D., Lin, Y.-H., 2016. Assessing the oxidative potential of isoprene-derived epoxides and secondary organic aerosol. Atmos. Environ. 130, 211–218.

Laskin, A., Laskin, J., Nizkorodov, S.A., 2015. Chemistry of atmospheric Brown carbon. Chem. Rev. 115, 4335–4382.

Li, X., Kuang, X.M., Yan, C., Ma, S., Paulson, S.E., Zhu, T., Zhang, Y., Zheng, M., 2019a. Oxidative potential by $PM_{2.5}$ in the north China plain: generation of hydroxyl radical. Environ. Sci. Technol. 53, 512–520.

Li, Z., Nizkorodov, S.A., Chen, H., Lu, X., Yang, X., Chen, J., 2019b. Nitrogen-containing secondary organic aerosol formation by acrolein reaction with ammonia/ammonium. Atmos. Chem. Phys. 19, 1343–1356.

Lin, P., Huang, X.-F., He, L.-Y., Zhen Yu, J., 2010. Abundance and size distribution of HULIS in ambient aerosols at a rural site in South China. J. Aerosol Sci. 41, 74–87.

Lin, P., Rincon, A.G., Kalberer, M., Yu, J.Z., 2012. Elemental composition of HULIS in the Pearl River Delta Region, China: results inferred from positive and negative electrospray high resolution mass spectrometric data. Environ. Sci. Technol. 46, 7454–7462.

Lin, P., Yu, J.Z., 2011. Generation of reactive oxygen species mediated by humic-like substances in atmospheric aerosols. Environ. Sci. Technol. 45, 10362–10368.

Lin, M., Yu, J.Z., 2019. Effect of metal-organic interactions on the oxidative potential of mixtures of atmospheric humic-like substances and copper/manganese as investigated by the dithiothreitol assay. Sci. Total Environ. 697, 134012.

Lin, M., Yu, J.Z., 2020. Assessment of interactions between transition metals and atmospheric organics: ascorbic acid depletion and hydroxyl radical formation in organic-metal mixtures. Environ. Sci. Technol. 54, 1431–1442.

Lu, S., Win, M.S., Zeng, J., Yao, C., Zhao, M., Xiu, G., Lin, Y., Xie, T., Dai, Y., Rao, L., Zhang, L., Yonemochi, S., Wang, Q., 2019. A characterization of HULIS-C and the oxidative potential of HULIS and HULIS-Fe(II) mixture in $PM_{2.5}$ during hazy and non-hazy days in Shanghai. Atmos. Environ. 219, 117058.

Lyu, Y., Guo, H.B., Cheng, T.T., Li, X., 2018. Particle size distributions of oxidative potential of lung-deposited particles: assessing contributions from quinones and water-soluble metals. Environ. Sci. Technol. 52, 6592–6600.

Ma, S.X., Ren, K., Liu, X.W., Chen, L.G., Li, M., Li, X.Y., Yang, J., Huang, B., Zheng, M., Xu, Z.C., 2015. Production of hydroxyl radicals from Fe-containing fine particles in Guangzhou, China. Atmos. Environ. Times 123, 72–78.

Ma, Y.Q., Cheng, Y.B., Qiu, X.H., Cao, G., Fang, Y.H., Wang, J.X., Zhu, T., Yu, J.Z., Hu, D., 2018. Sources and oxidative potential of water-soluble humic-like substances (HULISWS) in fine particulate matter ($PM_{2.5}$) in Beijing. Atmos. Chem. Phys. 18, 5607–5617.

Ma, Y., Cheng, Y., Qiu, X., Cao, G., Kuang, B., Yu, J.Z., Hu, D., 2019. Optical properties, source apportionment and redox activity of humic-like substances (HULIS) in airborne fine particulates in Hong Kong. Environ. Pollut. 255, 113087.

McWhinney, R.D., Badali, K., Liggio, J., Li, S.M., Abbatt, J.P., 2013. Filterable redox cycling activity: a comparison between diesel exhaust particles and secondary organic aerosol constituents. Environ. Sci. Technol. 47, 3362–3369.

Mudway, I.S., Stenfors, N., Duggan, S.T., Roxborough, H., Zielinski, H., Marklund, S.L., Blomberg, A., Frew, A.J., Sandstrom, T., Kelly, F.J., 2004. An in vitro and in vivo investigation of the effects of diesel exhaust on human airway lining fluid antioxidants. Arch. Biochem. Biophys. 423, 200–212.

Pang, H., Zhang, Q., Lu, X., Li, K., Chen, H., Chen, J., Yang, X., Ma, Y., Ma, J., Huang, C., 2019. Nitrite-mediated photooxidation of vanillin in the atmospheric aqueous phase. Environ. Sci. Technol. 53, 14253–14263.

Pope, C.A., Burnett, R.T., Thurston, G.D., Thun, M.J., Calle, E.E., Krewski, D., Godleski, J.J., 2004. Cardiovascular mortality and long-term exposure to particulate air pollution: epidemiological evidence of general pathophysiological pathways of disease. Circulation 109, 71–77.

See, S.W., Wang, Y.H., Balasubramanian, R., 2007. Contrasting reactive oxygen species and transition metal concentrations in combustion aerosols. Environ. Res. 103, 317–324.

Shen, H., Anastasio, C., 2011. Formation of hydroxyl radical from San Joaquin Valley particles extracted in a cell-free surrogate lung fluid. Atmos. Chem. Phys. 11, 9671–9682.

Son, Y., Mishin, V., Welsh, W., Lu, S.-E., Laskin, J.D., Kipen, H., Meng, Q., 2015. A novel high-throughput approach to measure hydroxyl radicals induced by airborne particulate matter. Int. J. Environ. Res. Publ. Health 12, 13678–13695.

Stone, E.A., Hedman, C.J., Sheesley, R.J., Shafer, M.M., Schauer, J.J., 2009. Investigating the chemical nature of humic-like substances (HULIS) in North American atmospheric aerosols by liquid chromatography tandem mass spectrometry. Atmos. Environ. 43, 4205–4213.

Sun, Y., Wang, Z., Fu, P., Jiang, Q., Yang, T., Li, J., Ge, X., 2013. The impact of relative humidity on aerosol composition and evolution processes during wintertime in Beijing, China. Atmos. Environ. 77, 927–934.

Tan, J., Xiang, P., Zhou, X., Duan, J., Ma, Y., He, K., Cheng, Y., Yu, J., Querol, X., 2016. Chemical characterization of humic-like substances (HULIS) in $PM_{2.5}$ in Lanzhou, China. Sci. Total Environ. 573, 1481–1490.

Tao, F., Gonzalez-Flecha, B., Kobzik, L., 2003. Reactive oxygen species in pulmonary

inflammation by ambient particulates. Free Radical Bio. Med. 35, 327–340.
Tuet, W.Y., Chen, Y., Xu, L., Fok, S., Gao, D., Weber, R.J., Ng, N.L., 2017. Chemical oxidative potential of secondary organic aerosol (SOA) generated from the photooxidation of biogenic and anthropogenic volatile organic compounds. Atmos. Chem. Phys. 17, 839–853.
Varga, B., Kiss, G., Ganszky, I., Gelencsér, A., Krivácsy, Z., 2001. Isolation of water-soluble organic matter from atmospheric aerosol. Talanta 55, 561–572.
Verma, V., Shafer, M.M., Schauer, J.J., Sioutas, C., 2010. Contribution of transition metals in the reactive oxygen species activity of PM emissions from retrofitted heavy-duty vehicles. Atmos. Environ. 44, 5165–5173.
Verma, V., Rico-Martinez, R., Kotra, N., King, L., Liu, J.M., Snell, T.W., Weber, R.J., 2012. Contribution of water-soluble and insoluble components and their hydrophobic/hydrophilic subfractions to the reactive oxygen species-generating potential of fine ambient aerosols. Environ. Sci. Technol. 46, 11384–11392.
Verma, V., Wang, Y., El-Afifi, R., Fang, T., Rowland, J., Russell, A.G., Weber, R.J., 2015. Fractionating ambient humic-like substances (HULIS) for their reactive oxygen species activity - assessing the importance of quinones and atmospheric aging. Atmos. Environ. 120, 351–359.
Vidrio, E., Jung, H., Anastasio, C., 2008. Generation of hydroxyl radicals from dissolved transition metals in surrogate lung fluid solutions. Atmos. Environ. 42, 4369–4379.
Vidrio, E., Phuah, C.H., Dillner, A.M., Anastasio, C., 2009. Generation of hydroxyl radicals from ambient fine particles in a surrogate lung fluid solution. Environ. Sci. Technol. 43, 922–927.
Visentin, M., Pagnoni, A., Sarti, E., Pietrogrande, M.C., 2016. Urban $PM_{2.5}$ oxidative potential: importance of chemical species and comparison of two spectrophotometric cell-free assays. Environ. Pollut. 219, 72–79.
Wang, Y., Hu, M., Lin, P., Guo, Q., Wu, Z., Li, M., Zeng, L., Song, Y., Zeng, L., Wu, Y., Guo, S., Huang, X., He, L., 2017. Molecular characterization of nitrogen-containing organic compounds in humic-like substances emitted from straw residue burning. Environ. Sci. Technol. 51, 5951–5961.
Wei, J., Yu, H., Wang, Y., Verma, V., 2019. Complexation of iron and copper in ambient particulate matter and its effect on the oxidative potential measured in a surrogate lung fluid. Environ. Sci. Technol. 53, 1661–1671.
Win, M.S., Tian, Z., Zhao, H., Xiao, K., Peng, J., Shang, Y., Wu, M., Xiu, G., Lu, S., Yonemochi, S., Wang, Q., 2018. Atmospheric HULIS and its ability to mediate the reactive oxygen species (ROS): a review. J Environ. Sci. China 71, 13–31.
Wu, G., Wan, X., Gao, S., Fu, P., Yin, Y., Li, G., Zhang, G., Kang, S., Ram, K., Cong, Z., 2018. Humic-like substances (HULIS) in aerosols of central Tibetan plateau (nam Co, 4730 m asl): abundance, light absorption properties, and sources. Environ. Sci. Technol. 52, 7203–7211.
Xiong, Q., Yu, H., Wang, R., Wei, J., Verma, V., 2017. Rethinking dithiothreitol-based particulate matter oxidative potential: measuring dithiothreitol consumption versus reactive oxygen species generation. Environ. Sci. Technol. 51, 6507–6514.
Yu, L., Smith, J., Laskin, A., Anastasio, C., Laskin, J., Zhang, Q., 2014. Chemical characterization of SOA formed from aqueous-phase reactions of phenols with the triplet excited state of carbonyl and hydroxyl radical. Atmos. Chem. Phys. 14, 13801–13816.
Yu, H., Puthussery, J.V., Verma, V., 2020. A semi-automated multi-endpoint reactive oxygen species activity analyzer (SAMERA) for measuring the oxidative potential of ambient $PM_{2.5}$ aqueous extracts. Aerosol Sci. Technol. 54, 304–320.
Zhang, X., Zhang, Y., Liu, Y., Zhao, J., Zhou, Y., Wang, X., Yang, X., Zou, Z., Zhang, C., Fu, Q., Xu, J., Gao, W., Li, N., Chen, J., 2019. Changes in the SO_2 level and $PM_{2.5}$ components in Shanghai driven by implementing the ship emission control policy. Environ. Sci. Technol. 53, 11580–11587.
Zhao, M., Qiao, T., Li, Y., Tang, X., Xiu, G., Yu, J.Z., 2016. Temporal variations and source apportionment of Hulis-C in $PM_{2.5}$ in urban Shanghai. Sci. Total Environ. 571, 18–26.
Zheng, G., He, K., Duan, F., Cheng, Y., Ma, Y., 2013. Measurement of humic-like substances in aerosols: a review. Environ. Pollut. 181, 301–314.